Silver-containing antimicrobial membrane based on chitosan-TPP hydrogel for the treatment of wounds

Pasquale Sacco · Andrea Travan · Massimiliano Borgogna · Sergio Paoletti · Eleonora Marsich

Accepted: 16 January 2015

Abstract Treatment of non-healing wounds represents hitherto a severe dilemma because of their failure to heal caused by repeated tissue insults, bacteria contamination and altered physiological condition. This leads to face huge costs for the healthcare worldwide. To this end, the development of innovative biomaterials capable of preventing bacterial infection, of draining exudates and of favoring wound healing is very challenging. In this study, we exploit a novel technique based on the slow diffusion of tripolyphosphate for the preparation of macroscopic chitosan hydrogels to obtain soft pliable membranes which include antimicrobial silver nanoparticles (AgNPs) stabilized by a lactose-modified chitosan (Chitlac). UV–Vis and TEM analyses demonstrated the time stability and the uniform distribution of AgNPs in the gelling mixture, while swelling studies indicated the hydrophilic behavior of membrane. A thorough investigation on bactericidal properties of the material pointed out the synergistic activity of chitosan and AgNPs to reduce the growth of *S. aureus*, *E. coli*, *S. epidermidis*, *P. aeruginosa* strains and to break apart mature biofilms. Finally, biocompatibility assays on keratinocytes and fibroblasts did not prove any harmful effects on the viability of cells. This novel technique enables the production of bioactive membranes with great potential for the treatment of non-healing wounds.

P. Sacco (✉) · A. Travan · M. Borgogna · S. Paoletti
Department of Life Sciences, University of Trieste, Via Licio Giorgieri 5, 34127 Trieste, Italy
e-mail: pasquale.sacco@phd.units.it

E. Marsich
Department of Medical, Surgical and Health Sciences, University of Trieste, Piazza dell'Ospitale 1, 34129 Trieste, Italy

1 Introduction

Topical wounds can be related to a defect or a break in the skin, resulting from physical or thermal damage and pathological conditions. Based on their nature and time-healing process, they can be classified as either acute or chronic [1]. The latter are lesions which fail to heal due to repeated tissue insults or altered physiological responses and range from diabetic ulcers to deep burns. Furthermore, chronic wounds are a fertile ground for bacteria proliferation [2, 3]. As a consequence, bacteria engage injured sites, enhance their proliferation and may cause the formation of complex surface-attached communities termed biofilms. Indeed, chronic wounds are an ideal environment for biofilm formation: the necrotic tissue and debris boost bacteria attachment (e.g. *Staphylococcus aureus* and *Pseudomonas aeruginosa*) and consequently lesions are susceptible to infection due to weakened host immune response [4]. James et al. demonstrated the presence of densely aggregated bacteria colonies surrounded by an extracellular matrix in human wounds: more in detail, 60 % of chronic wound and 6 % of acute wound specimens have proven hosting biofilm, thus suggesting that biofilms were most abundant in chronic wounds compared to acute lesions [5]. This condition affects negatively the physiological healing process and therefore leads to a decrease in life quality, to higher morbidity and mortality and to huge costs for the healthcare worldwide [6]. For instance, the cost related to non-healing ulcers has recently been estimated at 25 billion dollar annually in the United States [4].

Wound healing is a critical physiological process requiring absence of bacteria community in damaged sites [7]. Despite a broad range of antimicrobial agents as well as antibiotics (e.g. bacitracin, polymyxin B and neomycin) is commercially available [8], a successful tackling of

bacterial infections is particularly challenging due to an increase of microbial resistance caused by an abuse of such drugs [9].

Great importance is therefore given to the development of alternative antimicrobial agents and formulations able to avoid bacterial resistance while facilitating tissue repair. A recent review paper screened various methods aiming at eradicating bacteria infections including the use of heat, pressure, ultraviolet rays, antimicrobial nanoparticles, nanostructured surfaces, antibacterial peptides and cold atmospheric pressure plasma [10], but also the use of polycations (in particular both the native polysaccharide chitosan and its quaternarized ammonium derivative). Among these strategies, silver nanoparticles are widely considered as useful therapeutic agents for the prevention and eradication of wound colonization by microorganisms [11–13]. In the past, silver was employed to treat burns and chronic wounds [14]; moreover, several mixtures with sulfonamide were investigated [15]. Nowadays, nanocrystalline forms of silver can be prepared with variable size and shape by means of reliable methods including wet chemical synthesis and physical methods [8].

In a previous work, a 1-deoxylactit-1-yl chitosan, (shortly named "Chitlac"), was used for the in situ preparation of stable suspensions of evenly sized silver nanoparticles (AgNPs) [16], allowing to obtain an antimicrobial and biocompatible system for various biomedical applications [17–19].

A novel method, called "slow ion diffusion", was successfully devised to produce homogeneous macroscopic structures—such as membranes—using underivatized chitosan and the multicharged anion tripolyphosphate (TPP) [20]. In fact, the traditional technique of chitosan gelation with TPP unavoidable leads to the formation of hydrogel microspheres—which can not be used to obtain such products—due to an excess of uncontrolled point-like reactivity. On the other hand, preliminary experiments showed that Chitlac—a highly branched chitosan derivative—was practically unable to give tridimensional networks (gels) with the (oligomeric) anionic electrolyte TPP by exploiting ionotropic mechanisms. This is not surprising, given its—a priori unexpected—ability to give rise to stable binary solutions with anionic polysaccharides without polycation/polyanion coalescence, which was attributed to the reduced accessibility of the polycationic backbone due to branching [21, 22]. In addition, in the case of the interaction with TPP, an additional cause can be traced back to the too small amount of positive charges due to the unusual weak basicity of its secondary amines [23].

The present work is aimed at exploiting the newly proposed technique of homogeneous gelation of chitosan with TPP to entrap Chitlac-stabilized AgNPs for the preparation of hydrophilic antimicrobial membranes. The rationale of this approach is to enhance the antibacterial properties of the chitosan membrane by means of silver nanoparticles without impairing the viability of eukaryotic cells.

2 Materials and methods

2.1 Materials

Highly deacetylated chitosan (residual acetylation degree approximately 16 % as determined by means of ^{1}H-NMR), was purchased from Sigma-Aldrich (Chemical Co. USA). The relative molar mass ("molecular weight", MW) of chitosan determined by intrinsic viscosity measurements was found to be around 690,000 [24]. Chitlac (lactose-modified chitosan, CAS registry number 85941-43-1) was prepared according to the procedure reported elsewhere starting from highly deacetylated chitosan [24]. The composition of Chitlac was determined by means of ^{1}H-NMR and resulted to be: glucosamine residue 20 %, *N*-acetyl-glucosamine 18 % and 2-(lactit-1-yl)-glucosamine 62 %. The relative MW of Chitlac is around 1.5×10^{6}. Penta-sodium tripolyphosphate (TPP), sodium chloride (NaCl), glycerol (ReagentPlus® ≥ 99.0 %), silver nitrate ($AgNO_3$), ascorbic acid ($C_6H_8O_6$), MTT formazan powder [1-(4, 5-dimethylthiazol-2-yl)-3,5-diphenylformazan], phenazine methosulfate (PMS) powder and phosphate buffered saline (PBS) were all purchased from Sigma-Aldrich (Chemical Co. USA). Luria–Bertani (LB) broth, LB Agar and Brain Heart Infusion (BHI) broth were from Sigma-Aldrich (Chemical Co. USA). All other chemicals and reagents were of the highest purity grade commercially available.

2.2 Chitlac-silver nanoparticles preparation (Chitlac-nAg)

Although Chitlac is able to directly reduce silver ions [25], it was resorted to obtain silver nanoparticles (AgNPs) by reducing Ag^{+} ions by means of ascorbic acid in Chitlac solution according to the protocol described elsewhere [16]. Briefly, freeze-dried Chitlac was dissolved in deionized water to obtain a solution with final concentration 4 g L^{-1}. Chitlac solution was then mixed with $AgNO_3$ solution to achieve a final silver nitrate concentration of 4 mM. Ascorbic acid (reducing agent) solution was added at final concentration of 2 mM. Resulting mixture was held for 4 h at room temperature in dark condition and subsequently stored at 4 °C.

2.3 Membrane preparation

Membranes were produced by exploiting a controlled freeze-dried process starting from wall-to-wall hydrogels

obtained by a slow diffusion technique already described in [20]. Briefly, a solution composed by chitosan (2 % w/v), Chitlac-nAg (1.5 g L^{-1} and 1.5 mM as Chitlac and silver final concentration, respectively) and glycerol (5 % v/v)—"Chitlac-nAg gelling solution"—were casted into a mold (diameter = 22 mm, height = 2.5 mm) closed by two dialysis membranes (average flat width 33 mm, Sigma Aldrich, Chemical Co. USA) and fixed by double circular stainless iron rings. Glycerol was used as plasticizer. Mixture composed of chitosan (2 % w/v), Chitlac (1.5 g L^{-1}) and glycerol (5 % v/v) was employed for the preparation of membranes without AgNPs. The system was hermetically sealed and immersed into a TPP (1.5 % w/v)—NaCl (150 mM)—glycerol (5 % v/v) solution (Fig. 2b). Ions diffusion proceeded for 24 h under moderate stirring at room temperature allowing hydrogel formation. At the end of dialysis, hydrogels were washed twice in deionized water (1 h for each washing) in order to remove all residual traces of unbound TPP. Thereafter hydrogels were cooled by immersion in a liquid cryostat (circulating bath 28 L, VWR, Radnor, PA, USA). Ethylene glycol in water (3:1) was used as refrigerant fluid. Temperature was decreased from 20 to −20 °C by 5 °C steps with 20 min intervals. Samples were then freeze-dried for 24 h. For convenience, resulting membranes are named in overall manuscript as M (without AgNPs) and M-Ag (with AgNPs).

2.4 UV–Vis spectroscopy

UV–Visible spectroscopy measurements were performed on diluted (1:20) Chitlac-nAg gelling solution by means of Cary 400 spectrophotometer. Acetic acid (0.2 M) was used as blank solution and subsequently subtracted to all spectra recorded. The following setup was used throughout the measurements: data interval 1 nm, scan speed 600 nm min^{-1}.

2.5 Transmission electron microscopy (TEM)

TEM images were acquired by a PHILIPS EM 208 Microscope. Diluted (1:50) Chitlac-nAg gelling solution was deposited onto Nickel grids coated with a carbon film and dried overnight. Images were recorded at different magnification. Statistical analysis was performed upon 140 silver nanoparticles randomly selected at 89 kX magnification. The diameter of silver nanoparticles was calculated by ImageJ software.

2.6 Morphological analyses

Morphological analyses of hydrogels embedding silver nanoparticles and of M-Ag membranes were performed by scanning electron microscopy (Quanta250 SEM, FEI, Oregon, USA). In environmental conditions (E-SEM), hydrated specimens were mounted on aluminium stubs covered with two sides conductive carbon adhesive tape. In the case of cross-section evaluation, samples were cut in parallel to the cylinder axis and then prepared as described above. Samples were then analyzed in secondary electron detection mode. The working distance was adjusted in order to obtain the suitable magnification. Freeze-dried membranes were sectioned and directly visualized after sputter-coating with an ultrathin layer of gold. The accelerating voltage was kept constant at 30 kV.

2.7 Swelling studies

Swelling studies of M-Ag membranes were carried out placing samples in 10 mL of PBS (pH 7.4) up to 3 days at 37 °C. At different time intervals (t = 0, 2, 4, 6, 8, 24, 48 and 72 h) membranes were removed from the medium and weighed after blotting the excess of water using filter paper. The swelling ratio was calculated as the percentage of water uptake with respect to the initial weight in agreement with the following formula:

$$Water\ uptake = (W_t - W_0)/W_0$$

where W_t is the weight of samples at different time intervals and W_0 the dry weight of membranes at t = 0. All measurements were performed in triplicate.

2.8 Antimicrobial tests

The antibacterial activity of both M and M-Ag membranes was evaluated using strains of *Escherichia coli* (ATCC® 25922™), *Staphylococcus epidermidis* (ATCC® 12228™), *Staphylococcus aureus* (ATCC® 25923™) and *Pseudomonas aeruginosa* (ATCC® 27853™).

2.8.1 Growth inhibition assay

Membranes were sterilized (30 min of UV-irradiation for each side of sample) and incubated in sterilized PBS for 72 h at 37 °C under shaking condition in order to re-swell the system. Bacterial suspensions were prepared by adding 20 µL of bacteria, preserved in glycerol, to 5 mL of LB broth. The obtained suspensions were incubated overnight at 37 °C. After 24 h, 500 µL of bacterial suspension was diluted in 10 mL of broth and grown up for 90 min at 37 °C in order to restore an exponential growth phase. Bacterial concentration was measured by means of optical density (OD) at 600 nm. The bacterial suspension was then diluted in 10 % (v/v) LB broth in PBS to obtain a final concentration of 5×10^6 bacteria mL^{-1}. After re-swelling, PBS was removed from membranes and 2 mL of bacterial suspension was added to each one. All bacteria strains were

then incubated at 37 °C for 4 h. Tests were carried out in shaking condition (140 rpm) to optimize the contact between bacteria and membranes. At the end of incubation, bacterial suspension was collected and membranes were washed with 2 mL of PBS by vortexing for defined time so as to recover all bacteria. The washing solution was then added to the bacterial suspension previously transferred into a tube. The total collected bacterial solution was serially diluted in PBS (from 10^{-1} to 10^{-5}) and 25 µL of each suspension were plated on LB agar. After overnight incubation at 37 °C, the colony forming units (CFU) were counted. Outcomes were compared with a suspension of bacteria grown in liquid medium as control. Data are pointed out as the mean of three independent determinations with comparable results.

2.8.2 *Biofilm formation*

Bacterial suspensions of *S. aureus* and *P. aeruginosa* were prepared by adding 20 µL of bacteria, preserved in glycerol, to 5 mL of BHI broth *plus* 3 % w/v sucrose. The obtained suspensions were incubated overnight at 37 °C. After 24 h, bacteria were diluted 1:100 in the same broth and plated (300 µL/well) into 24-well plates. For confocal laser scanning microscopy analyses, bacteria were plated on sterile 13 mm tissue culture coverslips (Sarstedt, USA) previously laid down on the bottom of culture plate wells. Plates were incubated at 37 °C for 24 h allowing biofilm formation After 24 h, broth was removed and formed biofilm was carefully rinsed twice with 100 µL of sterile PBS in order to remove non-adherent cells. 300 µL of PBS were then added to each well and circular specimens of swollen membranes were deposited on the bacterial layer. Biofilms treated with membranes were then incubated at 37 °C and MTT assay was performed according to the following protocol after 4 and 24 h of incubation.

2.8.3 *Viable biomass assessment*

The test was performed according to the protocol described elsewhere [26]. Briefly, MTT stock solution was prepared by dissolving 5 mg mL^{-1} of MTT powder in sterile PBS. PMS stock solution was prepared by dissolving 0.3 mg mL^{-1} of relative powder in sterile PBS. Solutions were further filtered (0.22 µm filters, Biosigma, Italy) and stored at 2 °C in light-proof vials until the day of the experiment, when a fresh measurement solution (FMS) was prepared by mixing 0.5 mL of MTT stock solution, 0.5 mL of PMS stock solution, and 4 mL of sterile PBS. DMSO was used as lysing solution (LS). After the biofilm incubation period, membranes and PBS were gently removed from the plates and each well was carefully rinsed three times with 100 µL of sterile PBS in order to remove non-adherent cells. 200 µL of FMS solution were placed into each well and the plates were incubated for 3 h under light-proof conditions at 37 °C. The FMS solution was then gently removed and formazan crystals were dissolved by adding 200 µL of LS to each well. Plates were stored for an additional 1 h under light-proof conditions at room temperature and then 80 µL of the solution were transferred into the wells of 96-well plates. The absorbance of the solution was measured using a spectrophotometer (Infinite M200 PRO NanoQuant, Tecan) at a wavelength of 550 nm. Outcomes were expressed as OD units and are the mean of three independent experiments.

2.9 Confocal laser scanning microscopy (LSCM)

LSCM studies were addressed at detecting viability/death of bacteria grown in the biofilm community. FilmTracer Live/Dead biofilm viability kit (Invitrogen™) was used. Dead cells were stained by propidium iodide, (red fluorescence—λ_{ex} 514 nm; λ_{em} 590 nm) whereas live cells by SYTO® 9 (green fluorescence—λ_{ex} 488 nm; λ_{em} 515 nm). Staining was performed on biofilms grown on coverslips as described above, according to the manufacture's protocol. Images were acquired on a Nikon Eclipse C1si confocal laser scanning microscope with a Nikon Plan Fluor 20X as objective. Resulting stacks of images were analyzed using ImageJ software.

2.10 Cell culture

Mouse fibroblast-like NIH-3T3 (ATCC® CRL1658) and immortalized human keratinocyte HaCaT (kindly gifted by Dr. Chiara Florio, University of Trieste) cell lines were used for the in vitro experiments. Both cell lines were cultured in Dulbecco's Modified Eagle's Medium high glucose (EuroClone, Italy), 10 % heat-inactivated fetal bovine serum (Sigma Aldrich, Chemical Co. USA), 100 U mL^{-1} penicillin, 100 µg mL^{-1} streptomycin and 2 mM L-glutamine in a humidified atmosphere of 5 % CO_2 at 37 °C.

2.11 Cytotoxicity evaluation and fluorescence microscopy

In vitro cytotoxicity of membranes was evaluated by using MTT assay on both NIH-3T3 and HaCaT cells. UV-sterilized samples of approximately 20 mm in diameter and 1.5 mm in width were placed in Dulbecco's modified Eagle's medium, inactivated fetal bovine serum 10 %, penicillin 100 U mL^{-1}, streptomycin 100 µg mL^{-1} and L-glutamine 2 mM for 72 h at 37 °C and 5 % pCO_2. After 72 h of incubation, the cytotoxicity test was performed by direct contact of the cells with the swollen membranes. 200,000 cells were plated on 6-well plates and, after

complete adhesion, culture medium was changed with 2 mL of fresh medium. Tested materials were directly deposited on the cell layer. After 24 and 72 h, MTT assay was performed according to the manufacture's protocol. As a positive control material, poly(urethane) films containing 0.25 % zinc dibuthyldithiocarbamate (ZDBC) (20 mm disks) were used. As negative control material, plastic poly(styrene) sheets (20 mm disks) were used. Each material test was performed in triplicate. Cytotoxicity was expressed as percentage of viability by normalizing the $OD_{570\ nm}$ of samples to the $OD_{570\ nm}$ of the negative control. Data are pointed out as the mean of three independent determinations with comparable results.

For fluorescence microscopy analyses, cells were fixed by 4 % paraformaldehyde in PBS, permeabilized with 0.1 % v/v Triton X-100 and blocked with 1 % BSA (15 min at 37 °C). Finally, cells were stained 1 h at 37 °C with Phalloidin-FITC 50 µg mL^{-1} and 1 min with DAPI 0.1 µg mL^{-1} (Sigma-Aldrich, Chemical Co. USA). Photographs were taken with a Nikon Eclipse E600 microscope equipped with a Nikon Coolpix995 digital camera.

2.12 Statistical analyses

Data are expressed as means and standard deviations (SD). Statistical analyses were performed using Student's *t* test, and a *P* value of < 0.05 was considered statistically significant.

3 Results

3.1 Stability and dispersion of silver nanoparticles

The first part of this work was addressed to evaluate the dispersion and the stability of silver nanoparticles in the Chitlac-nAg gelling solution. UV–Vis spectroscopy and TEM investigations were performed to evaluate shape, distribution and dimensions of the nanoparticles. Figure 1a

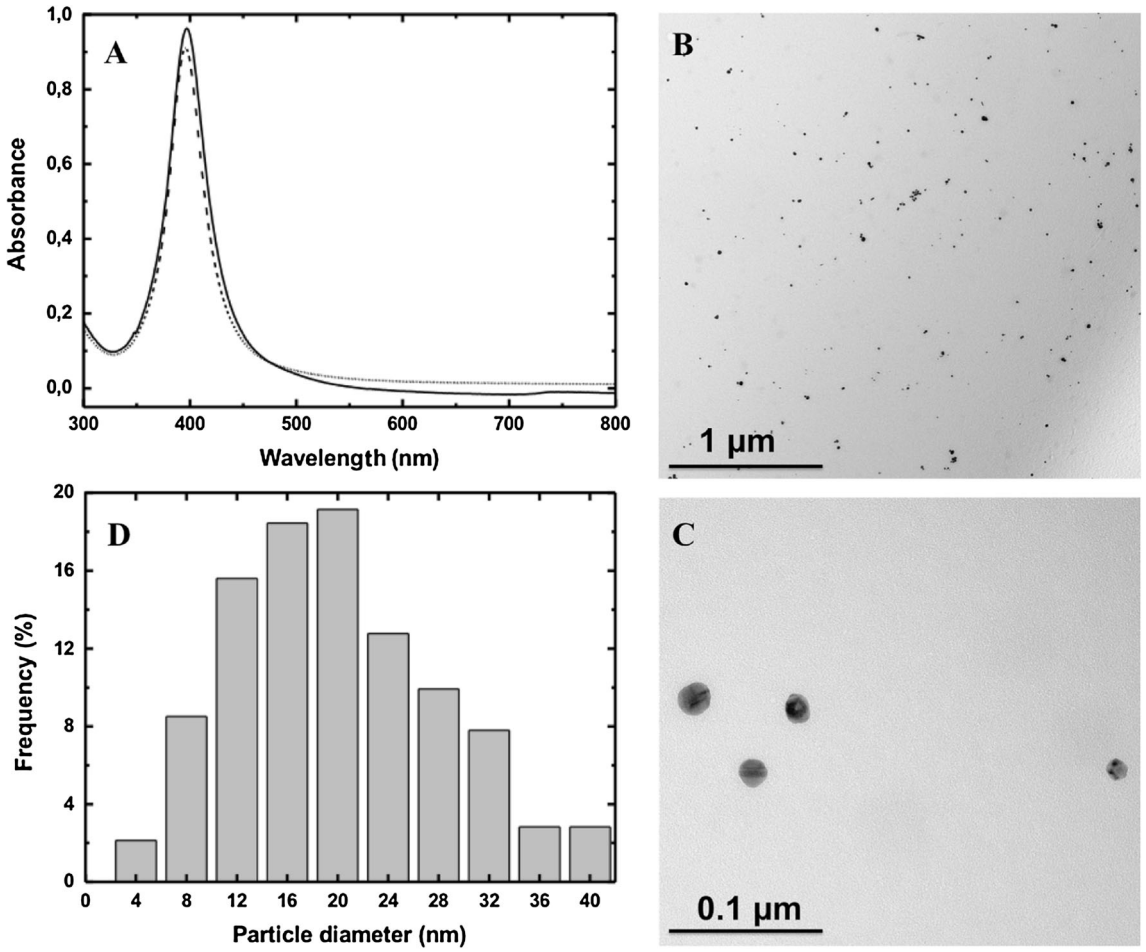

Fig. 1 **a** UV–Vis spectra of silver nanoparticles in diluted 1:20 Chitlac-nAg gelling solution (chitosan, Chitlac-nAg, glycerol) after 1 day (*solid line*) and after 5 months storage (*dashed line*). **b**, **c** TEM images of silver nanoparticles dispersed in diluted 1:50 Chitlac-nAg gelling solution at different magnifications. **d** Silver nanoparticles size distribution based on TEM images and calculated by means of ImageJ software

shows the UV–Vis spectra of diluted Chitlac-nAg gelling solution pointing out the plasmon resonance band at about 400 nm due to the presence of the AgNPs. The symmetrical shape of this narrow band suggests that the nanoparticles are well dispersed and stabilized in the Chitlac solution. No significant differences in the UV–Vis spectra were observed after 5 months of storage at room temperature, indicating a good stability over time of the colloidal mixture.

In order to evaluate nanoparticles shape and dimensions, TEM analyses were carried out. Figure 1b, c displays images of the nanoparticles in diluted Chitlac-nAg gelling solution at different magnifications, showing good dispersion, lack of aggregates and spherical shape morphology for the majority of nanoparticles. TEM images have been analyzed to evaluate the dimensional distribution of the nanoparticles. The histogram in Fig. 1d points out a narrow size distribution scattered with maximum frequency at around 20 nm and a mean diameter of 20.1 ± 8.4 nm.

3.2 Preparation of membranes

Chitlac-nAg was mixed with chitosan (and glycerol) and a homogeneous solution was obtained. A sketch of the interpenetrated polymer network preparation is depicted in Fig. 2a, where Chitlac and chitosan are represented as worm-like structures whereas silver nanoparticles as red dots. This mixture was confined in dialysis membranes by means of a custom-made vessel immersed in a TPP solution (Fig. 2b) [20]. This technique enabled to turn the Chitlac-nAg gelling solution into a macroscopic homogenous hydrogel, exploiting the slow TPP diffusion through the dialysis membranes (Fig. 3a). E-SEM images pointed out the continuous polymeric network both at the surface and at the cross-section of the hydrogel (Fig. 3b, c). Since the primary purpose of the present work was to produce dried pliable membranes, the nanocomposite hydrogels were freeze-dried according to a procedure previously described [20]. The resulting membrane (Fig. 3d) was analyzed by SEM analyses that revealed the compact polymeric mesh of the material (Fig. 3e, f).

3.3 Antibacterial properties

Antibacterial features of the membranes were evaluated towards both $Gram^-$ and $Gram^+$ bacteria strains. Experiments were addressed to assess the bacterial growth inhibition and biofilm eradication activities of the membranes with AgNPs (M-Ag) in comparison with the membranes without AgNPs (M). Figure 4a, b shows the results obtained by a growth inhibition assay with *E. coli* and *S. aureus*. For both strains, a significant drop of CFU ($P < 0.001$) was identified for both M- and M-Ag-treated samples in comparison with control (suspension of bacteria grown in medium). M membranes exert mainly a bacteriostatic effect which can be ascribed to the presence of chitosan. Indeed, the number of bacteria after four hours remains basically constant when compared with the amount of bacteria seeded at time zero (5×10^6 bacteria mL^{-1}). At variance, M-Ag membranes showed a marked antibacterial activity in comparison with M ones ($P < 0.001$) owing to the presence of embedded AgNPs. This finding is confirmed by visual observations as reported in Fig. 4e–j that show the growth of *E. coli* colonies on LB agar for treated and untreated samples. A similar trend was observed for *P. aeruginosa* (Fig. 4c) where a drop of around 5 Log was found for M-Ag-treated samples. Also in this case, the presence of AgNPs in M-Ag membranes enables to significantly increase ($P < 0.05$) the antibacterial properties of such membranes towards M ones. In the case of *S. epidermidis*, no significant differences were revealed between M and M-Ag after 4 h of treatment,

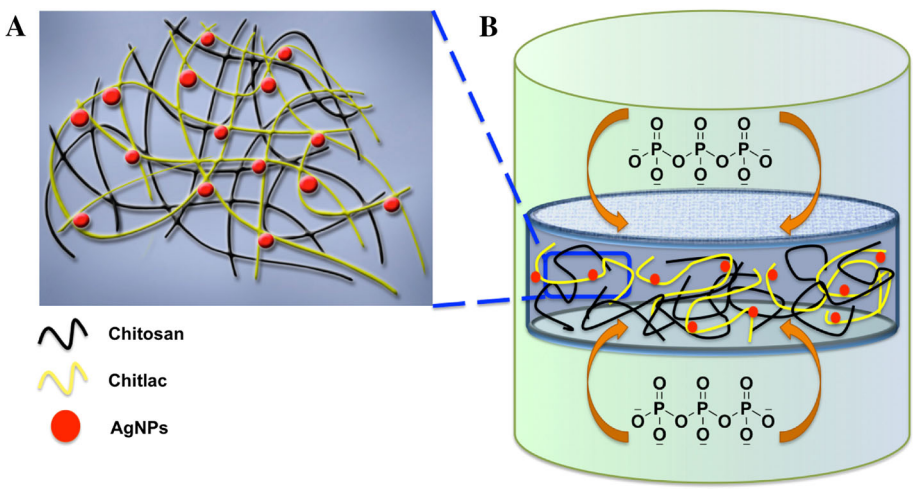

Fig. 2 **a** Entangled distribution of chitosan (*black ribbons*), Chitlac (*yellow ribbons*) and AgNPs (*red dots*) in Chitlac-nAg gelling solution. **b** Slow ion diffusion technique: a vessel containing a viscous Chitlac-nAg gelling solution is placed into an outer solution [TPP (1.5 % w/v)—NaCl (150 mM)—glycerol (5 % v/v)] under stirring. When the dialysis starts, TPP ions diffuse through the semipermeable walls (membranes) of the vessel so as to favor a controlled ionotropic gelation (Color figure online)

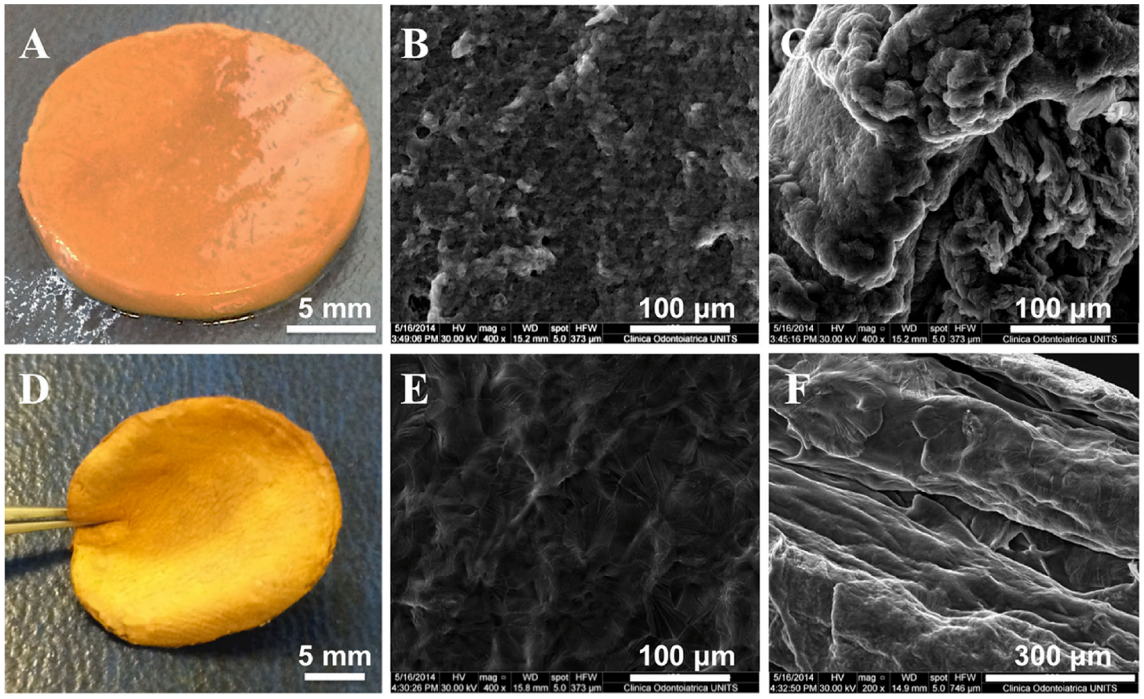

Fig. 3 *Upper row* hydrogel embedding AgNPs. **a** Top view, **b** E-SEM micrograph of the hydrogel surface, **c** E-SEM micrograph of the hydrogel cross-section. *Lower row* dried membrane derived from the hydrogel depicted in (**a**) by freeze-drying. **d** Top view, **e** SEM micrograph of the membrane surface, **f** SEM micrograph of the membrane cross-section

although a marked antibacterial activity (3 Log CFU drop) was detected for both of them compared with the control (data not shown). In order to spot significant differences between M and M-Ag membranes with this strain, time of incubation was increased up to 20 h so as to extend the exposure time of bacteria to membranes. In these conditions, the Log CFU mL^{-1} calculated for M-Ag and M membranes were 1.9 ± 0.2 and 3.3 ± 0.6, respectively ($P < 0.05$, $n = 3$), thus indicating an enhanced activity in the presence of AgNPs (Fig. 4d).

After demonstrating that M-Ag membranes possess the capability to significantly impair the growth of different bacteria strains, the following step was to verify the activity of such membranes upon mature biofilms. Figure 5a, b pointed out the results obtained after 4 and 24 h of treatment for *S. aureus* and *P. aeruginosa* biofilms, respectively. In the case of the $Gram^+$ strain, it was revealed that M-Ag membranes were effective in breaking apart the biofilm, as revealed by MTT colorimetric assay where samples treated with membranes embedding AgNPs showed a reduction of about 75 % of OD after only 4 h with respect to control (Fig. 5a). Conversely, M membranes did not impair biofilm viability in the same timeframe. At longer time (24 h of treatment), M membranes displayed an antibacterial activity towards *S. aureus* biofilm, in any case milder than in the presence of AgNPs (M-Ag). These results were confirmed by analysis of the biofilms with confocal laser scanning microscopy (Fig. 5c–e). In Fig. 5e *S. aureus* biofilm appears as a green fluorescent layer, which indicates the good bacteria viability in the case of the growth control. Conversely, cells treated for 24 h with M-Ag membranes pointed out mainly red fluorescent bacteria and only a few green cells, thus suggesting cell membrane damage and the consequent entry of propidium iodide into dead cells (Fig. 5d). Moreover, the bacteria layer appeared non-homogeneous and broken apart. Biofilms treated with M membranes showed a partial disaggregation of the bacteria layer after 24 h of treatment, as pointed out by sagittal YZ projection, albeit a higher number of viable cells with respect to M-Ag-treated biofilm was detected (Fig. 5c). These findings are in agreement with what measured in the viable biomass experiments above discussed. Viable biomass assessment was also carried out on *P. aeruginosa* as shown in Fig. 5b. In this case, by comparing M and M-Ag membranes no statistical differences were observed at investigated times, even if a OD decrease was measured for both in comparison with the control group.

3.4 Swelling studies

Swelling behavior of M-Ag membranes is shown in Fig. 6. Membranes demonstrated a complete swelling

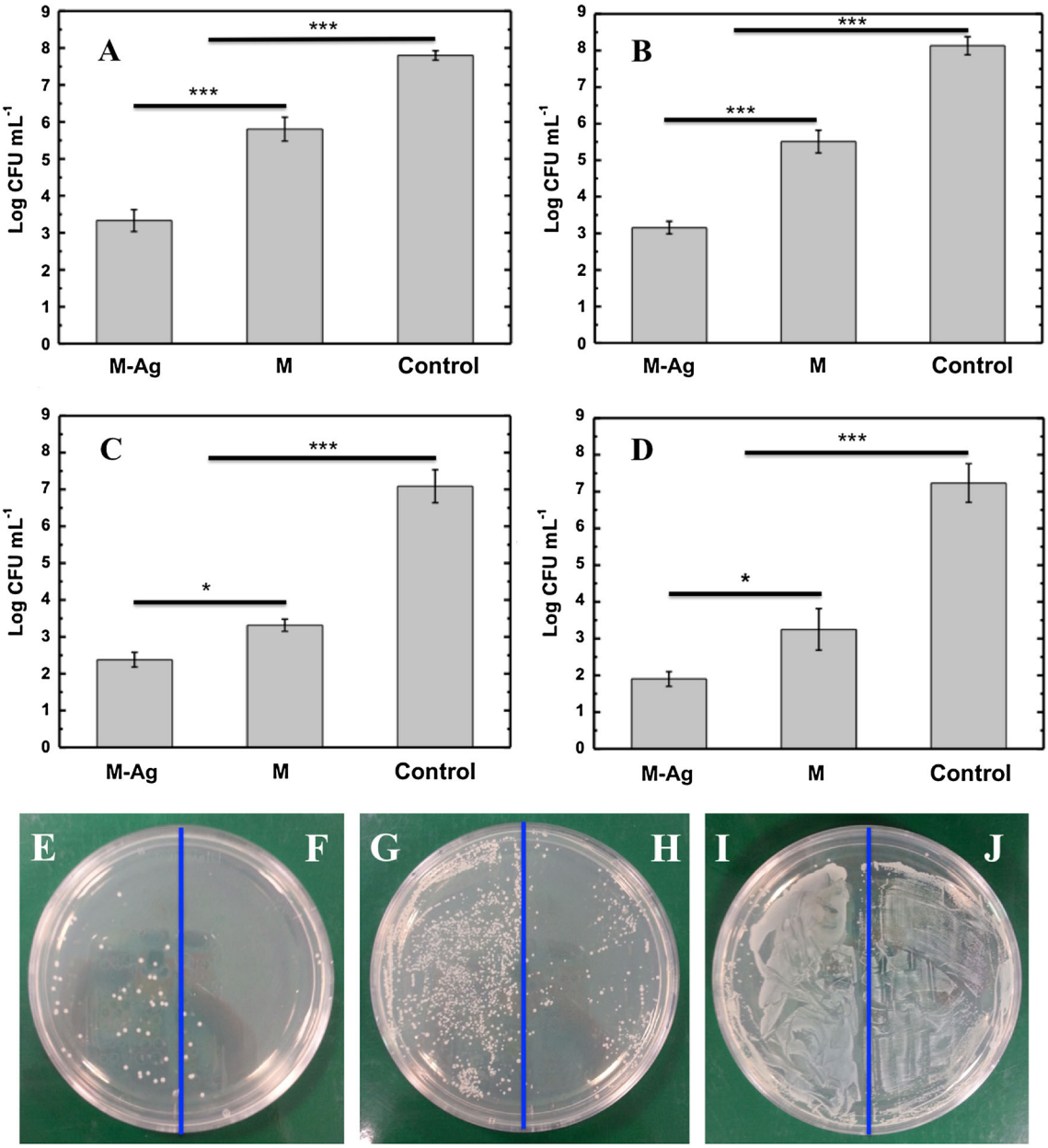

Fig. 4 Growth inhibition rate expressed as Log CFU mL^{-1} of *E. coli* (**a**), *S. aureus* (**b**) and *P. aeruginosa* (**c**) following 4 h of treatment with M-Ag (with AgNPs) and M (without AgNPs) membranes. Growth inhibition rate of *S. epidermidis* (**d**) following 20 h of treatment with the same membranes. Statistical differences were determined by means of Student's *t* test. $^{*}P < 0.05$; $^{**}P < 0.01$; $^{***}P < 0.001$. *E. coli* colonies on LB agar: not diluted (**e**) and diluted 10^{-1} (**f**) M-Ag-treated sample; not diluted (**g**) and diluted 10^{-1} (**h**) M-treated sample; not diluted (**i**) and diluted 10^{-1} (**j**) control sample

state in PBS buffer at 37 °C after 72 h of soaking. The plot displays a slow, albeit constant, water uptake by membranes that took place in the first 4 h. Furthermore, the water uptake increased from 34.1 ± 5.6 to 191.7 ± 29.8 % after 48 h of soaking because of diffusion of water molecules into the hydrophilic polymeric network. As a result, membranes reached the equilibrium and the swelling rate did not vary significantly after 72 h (193.6 ± 28.8 % as final water uptake).

3.5 Biocompatibility

In order to assess the biocompatibility of M-Ag membranes for potential dermatological applications, MTT assay was performed on keratinocytes (HaCaT) and fibroblasts (NIH-3T3) cell lines and results are pointed out in Fig. 7. M membranes were tested as chitosan-based control without AgNPs. Plot in Fig. 7a shows that the viability of treated HaCaT cells was not influenced when membranes are in

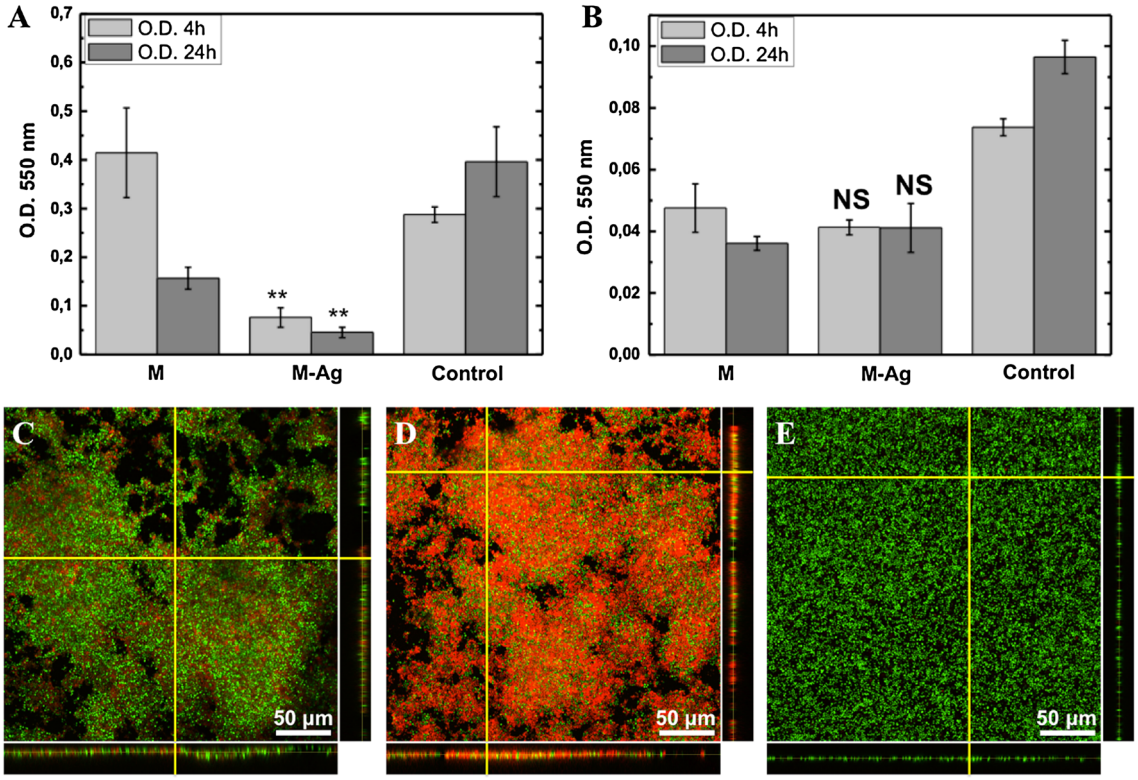

Fig. 5 Viable biomass MTT assay expressed as OD at 550 nm of *S. aureus* (**a**) and *P. aeruginosa* (**b**) following 4 and 24 h of treatment with M-Ag (with AgNPs) and M (without AgNPs) membranes. Statistical differences were determined by means of Student's *t* test. *NS* no statistical differences versus M; $^{**}P < 0.01$ versus M. LSCM images of *S. aureus* biofilm: M-treated sample after 24 h (**c**), M-Ag 24 h-treated sample (**d**) and control (**e**). For all images *green fluorescence* indicates live cells whereas *red fluorescence* refers to dead ones. Horizontal sagittal sections: XZ projections; vertical sagittal sections: YZ projections (Color figure online)

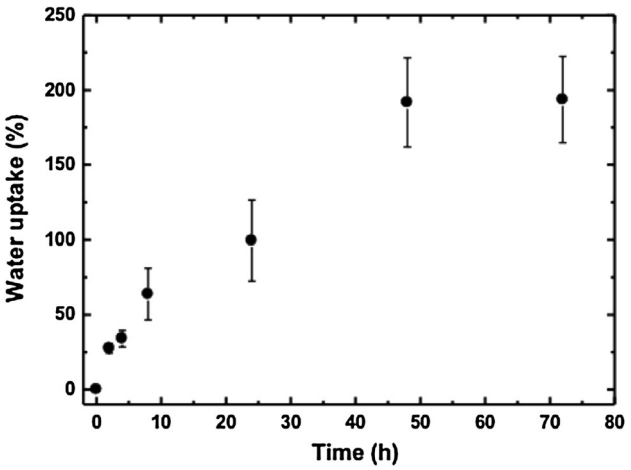

Fig. 6 Water uptake (%) versus time (h) of M-Ag membranes immersed in PBS buffer (pH 7.4) at 37 °C. The data are expressed as mean (±SD) of three samples

direct contact with cells. No statistical differences were identified for M-Ag samples compared to the negative control at time investigated, thus suggesting lack of cytotoxicity of the material. This outcome is consistent with what observed by optical microscopy (Fig. 7c), where cells showed a normal keratinocyte-like morphology, good spreading, and absence of suffering signals such as cytoplasmic vacuoles, chromatin aggregation, or formation of cellular debris. Fluorescence microscopy (Fig. 7d) confirmed the viability of treated cells showing an optimal distribution of cytoskeleton (Phalloidin-FITC staining) and intact nuclei (DAPI staining). Moreover, the increase of fluorescence from 24 to 72 h suggested a higher number of viable cells (data not shown). Similar results were obtained with NIH-3T3 cell line as shown in Fig. 7b. Also in this case the MTT assay did not point out any significant difference between treated samples versus negative control and optical/fluorescence microscopy confirmed the viability of cells (Fig. 7e, f).

4 Discussion

The main goal of this work traced back to the idea of exploiting the ability of two polysaccharides, namely chitosan and Chitlac, to form antibacterial and non-cytotoxic hydrophilic membranes to be used as dressing in the

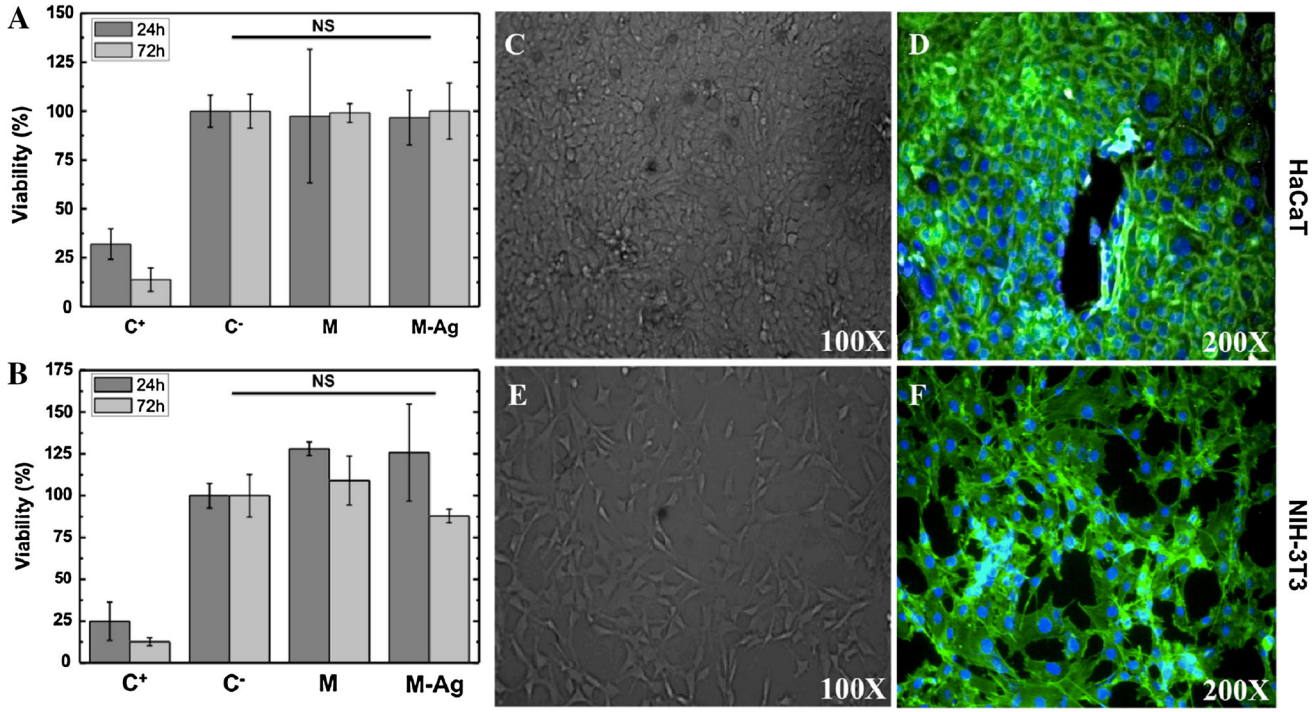

Fig. 7 Percentage of viability of keratinocytes HaCaT (**a**) and fibroblast NIH-3T3 (**b**) cells measured using MTT assay. M-Ag (with AgNPs) and M (without AgNPs) membranes were kept in touch with cells and test was performed after 24 and 72 h of treatment. Poly(urethane) sheets containing 0.25 % zinc dibuthyldithiocarbamate were used as contact positive control (C^+) whereas plastic poly(styrene) sheets were used as contact negative control (C^-). Statistical differences were determined by means of Student's *t* test *NS* no statistical differences between C^- and M-Ag both at 24 and 72 h of treatment. Optical microscopy of HaCaT (**c**) and NIH-3T3 (**e**) cell lines after 72 h of treatment with M-Ag membrane. Fluorescence microscopy of HaCaT (**d**) and NIH-3T3 (**f**) cell lines: cytoskeleton was stained by means of Phalloidin-FITC (P-FITC) whereas nuclei by DAPI. Images were acquired after 72 h of contact with M-Ag membranes

treatment of non-healing wounds. In a previous work, the higher ability of Chitlac to coordinate and stabilize silver nanoparticles compared to chitosan was demonstrated [16]. In a recent study, we described a novel process to exploit the capability of chitosan to undergo ionotropic gelation in the presence of TPP anions [20]. Given these premises, our aim was to create a chitosan–Chitlac-nAg blend capable of gelling in the presence of TPP without affecting the stability and the antibacterial activity of silver nanoparticles. When the Chitlac-nAg colloidal dispersion and chitosan solution were mixed at investigated concentrations, no aggregates or precipitates were observed, thus suggesting the completely miscibility of the two polysaccharides. TEM analyses demonstrated the presence of small, round-shaped and mono-dispersed nanoparticles (Fig. 1b, c). This result was supported by UV–Vis measurements where the presence of very narrow and symmetrical bands confirmed the good dispersion of nanoparticles. This finding clearly suggests that the presence of chitosan-glycerol did not negatively affect the stability of silver nanoparticles coordinated by Chitlac. In this study, Chitlac-nAg showed not to hamper the ionotropic gelation of chitosan, which resulted in homogeneous hydrogels and membranes as confirmed by SEM investigation (Fig. 3a–f).

An ideal wound dressing should offer protection from infections, should remove wound exudates (maintaining at the same time a moist environment) and should demonstrate lack of cytotoxicity towards eukaryotic cells in order not to interfere with tissue regeneration [27]. According to these requirements, our studies were aimed at assessing the antibacterial properties of the membranes, their swelling behavior and the biocompatibility towards eukaryotic cells.

Anti-bacterial tests were carried out on *E. coli*, a typical bacterium employed in laboratory to assess the efficacy of antimicrobial agents and antibiotics, *S. epidermidis* which belongs to microbiota of the skin and finally *P. aeruginosa* and *S. aureus* because of their ability to produce biofilm in chronic wounds [4]. We demonstrated growth inhibition of all bacteria strains investigated by both M-Ag and M membranes (Fig. 4a–d). In detail, we proved the synergistic effect on bacteria killing of AgNPs when combined with chitosan after already 4 h of contact, considering that Chitlac is devoid of antibacterial properties [28]. In the case of *S. epidermidis*, statistical differences between

M-Ag and M membranes started to be evident only after longer times (20 h). The higher resistance of this strain towards silver nanoparticles is consistent with results obtained in our previous work [19].

The studies on mature biofilms pointed out that both membranes are able to break apart *S. aureus* biofilm after 24 h of treatment, as demonstrated by LSCM analyses (Fig. 5c, d). While M membranes are supposed to exert antibacterial activity owing to the properties of chitosan (electrostatic, hydrophobic and chelating effects [29]), M-Ag membranes also exploit the presence of silver nanoparticles to boost the bactericidal efficacy. This is confirmed by the rapid OD reduction already after 4 h of treatment in the case of *S. aureus* (Fig. 5a). It is very important to notice that LSCM images were acquired after removing membranes from the bacteria biofilm. Indeed, given that AgNPs was previously proved to exert its antibacterial activity by interaction with bacterial membranes [16, 30], in the present system we hypothesize that AgNPs grafted on the surface of M-Ag membranes interact with bacteria cells in correspondence to molecular target, e.g. thiol groups (–SH) of proteins, causing membrane damage [13, 30]. The bactericidal effect of silver in this system can be also ascribed to the small dimensions of the nanoparticles (20.1 ± 8.4 nm), which ensures a high surface area of contact with bacteria membranes [31].

Water uptake is particularly important for an ideal wound dressing because it enables to eliminate exudates from an infected lesion thus hampering bacteria spread. In this work, M-Ag membranes demonstrated the ability to uptake a large amount of water during 72 h of soaking (Fig. 6). This is in agreement with Silva et al. who demonstrated a similar water uptake in the case of tridimensional constructs based on chitosan [32]. Moreover, it is important to notice that membranes did not show dissolution in the medium and maintained their physical stability in the studied timeframe.

Concerning in vitro biocompatibility of the membranes, keratinocytes (HaCaT) and fibroblasts (NIH-3T3) cell lines were chosen because they are cellular components of skin and because of their large use as model to evaluate the response of biological systems towards biopolymer networks [33]. The MTT assay demonstrated lack of cytotoxicity both in the presence or absence of silver nanoparticles (Fig. 7a, b).

Tridimensional systems based on polysaccharide networks can prevent nanoparticles from being available for eukaryotic cellular uptake but, at the same time, preserve their antimicrobial activity allowing the direct interaction of the nanoparticles with the proteins localized on the bacterial surface [16]. In fact, in bacteria the thiol groups (–SH) of membrane proteins, main molecular targets of the silver antibacterial activity, are exposed to the extracellular portion of the membrane as discussed above.

Conversely to prokaryotic cells, eukaryotic cells do not have exterior (–SH) groups at membrane level [28]. As a result, AgNPs are unable to interact with them except if internalized. Indeed, recently Lee et al. proved that AgNPs were potentially cytotoxic towards NIH-3T3 cells when they were taken up, thus favoring changes of morphology, oxidative stress, induction of reactive oxygen species, up-regulation of Heme oxygenase 1 expression, apoptosis and autophagy [34]. Thanks to lack of morphological alterations and cellular debris in our model, as pointed out by optical and fluorescence microscopy, we tend to exclude a massive cellular uptake of silver nanoparticles, thus concluding they are firmly grafted and immobilized in the Chitlac/chitosan polymeric network and therefore do not diffuse into the surrounding environment. In the future, further studies will be devoted to confirm this hypothesis by estimating quantitatively the possible release of AgNPs from the membrane and to study the effects on immune system cells, macrophages and granulocytes.

5 Conclusions

In the present paper, a silver-containing antimicrobial membrane was prepared by means of a custom-made technique based on a slow ionotropic gelation of chitosan. This nanocomposite material was proved to possess antimicrobial activity towards bacteria suspensions and mature biofilms. The stability of Chitlac-coordinated AgNPs was not affected by mixture with chitosan and glycerol, enabling to prepare homogeneous macroscopic nanocomposite hydrogels and pliable membranes. Overall, the ability of AgNPs to enhance the antibacterial properties of chitosan, combined with the lack of cytotoxicity towards eukaryotic cell lines and the hydrophilic behavior of the construct, allow to consider this membrane as a promising biomaterial for the treatment of non-healing wounds.

Acknowledgments This study was supported by the Friuli-Venezia Giulia Regional Government (Project: "Nuovi biomateriali per terapie innovative nel trattamento delle ferite difficili"-LR 47/78). The financial support to P.S. (PhD position) by the Friuli-Venezia Giulia Regional Government and by the European Social Fund (S.H.A.R.M. project-Supporting human assets in research and mobility) is gratefully acknowledged. Miss Greta Galiussi and Dr. Renzo Menegazzi are thanked for their skillful assistance in the experimental part.

References

1. Boateng JS, Matthews KH, Stevens HNE, Eccleston GM. Wound healing dressings and drug delivery systems: a review. J Pharm Sci. 2008;97:2892–923.

2. Lee SJ, Heo DN, Moon J-H, Ko W-K, Lee JB, Bae MS, et al. Electrospun chitosan nanofibers with controlled levels of silver nanoparticles. Preparation, characterization and antibacterial activity. Carbohydr Polym. 2014;111:530–7.
3. Gawande PV, Leung KP, Madhyastha S. Antibiofilm and antimicrobial efficacy of DispersinB®-KSL-W peptide-based wound gel against chronic wound infection associated bacteria. Curr Microbiol. 2014;68:635–41.
4. Zhao G, Usui ML, Lippman SI, James GA, Stewart PS, Fleckman P, et al. Biofilms and inflammation in chronic wounds. Adv. Wound Care. 2013;2:389–99.
5. James GA, Swogger E, Wolcott R, deLancey Pulcini E, Secor P, Sestrich J, et al. Biofilms in chronic wounds. Wound Repair Regen. 2008;16:37–44.
6. Falanga V. The chronic wound: impaired healing and solutions in the context of wound bed preparation. Blood Cells Mol Dis. 2004;32:88–94.
7. Martin P. Wound healing–aiming for perfect skin regeneration. Science. 1997;276:75–81.
8. Gunasekaran T, Nigusse T, Dhanaraju MD. Silver nanoparticles as real topical bullets for wound healing. J Am Coll Clin Wound Spec. 2011;3:82–96.
9. Paphitou NI. Antimicrobial resistance: action to combat the rising microbial challenges. Int J Antimicrob Agents. 2013;42(Suppl): S25–8.
10. Mai-Prochnow A, Murphy AB, McLean KM, Kong MG, Ostrikov KK. Atmospheric pressure plasmas: infection control and bacterial responses. Int J Antimicrob Agents. 2014;43:508–17.
11. Reithofer MR, Lakshmanan A, Ping ATK, Chin JM, Hauser CAE. In situ synthesis of size-controlled, stable silver nanoparticles within ultrashort peptide hydrogels and their anti-bacterial properties. Biomaterials. 2014;35:7535–42.
12. Taglietti A, Arciola CR, D'Agostino A, Dacarro G, Montanaro L, Campoccia D, et al. Antibiofilm activity of a monolayer of silver nanoparticles anchored to an amino-silanized glass surface. Biomaterials. 2014;35:1779–88.
13. Madhumathi K, Sudheesh Kumar PT, Abhilash S, Sreeja V, Tamura H, Manzoor K, et al. Development of novel chitin/nanosilver composite scaffolds for wound dressing applications. J Mater Sci Mater Med. 2010;21:807–13.
14. Klasen H. A historical review of the use of silver in the treatment of burns, II. Renewed interest for silver. Burns. 2000;26:131–8.
15. Rai M, Yadav A, Gade A. Silver nanoparticles as a new generation of antimicrobials. Biotechnol Adv. 2009;27:76–83.
16. Travan A, Pelillo C, Donati I, Marsich E, Benincasa M, Scarpa T, et al. Non-cytotoxic silver nanoparticle-polysaccharide nanocomposites with antimicrobial activity. Biomacromolecules. 2009;10:1429–35.
17. Marsich E, Travan A, Donati I, Turco G, Kulkova J, Moritz N, et al. Biological responses of silver-coated thermosets: an in vitro and in vivo study. Acta Biomater. 2013;9:5088–99.
18. Nganga S, Travan A, Marsich E, Donati I, Söderling E, Moritz N, et al. In vitro antimicrobial properties of silver-polysaccharide coatings on porous fiber-reinforced composites for bone implants. J Mater Sci Mater Med. 2013;24:2775–85.
19. Marsich E, Bellomo F, Turco G, Travan A, Donati I, Paoletti S. Nano-composite scaffolds for bone tissue engineering containing silver nanoparticles: preparation, characterization and biological properties. J Mater Sci Mater Med. 2013;24:1799–807.
20. Sacco P, Borgogna M, Travan A, Marsich E, Paoletti S, Asaro F, et al. Polysaccharide-based networks from homogeneous chitosan-tripolyphosphate hydrogels: synthesis and characterization. Biomacromolecules. 2014;15:3396–405.
21. Donati I, Borgogna M, Turello E, Cesàro A, Paoletti S. Tuning supramolecular structuring at the nanoscale level: nonstoichiometric soluble complexes in dilute mixed solutions of alginate and lactose-modified chitosan (chitlac). Biomacromolecules. 2007;8:1471–9.
22. Donati I, Haug IJ, Scarpa T, Borgogna M, Draget KI, Skjåk-Braek G, et al. Synergistic effects in semidilute mixed solutions of alginate and lactose-modified chitosan (chitlac). Biomacromolecules. 2007;8:957–62.
23. D'Amelio N, Esteban C, Coslovi A, Feruglio L, Uggeri F, Villegas M, et al. Insight into the molecular properties of Chitlac, a chitosan derivative for tissue engineering. J Phys Chem B. 2013;117:13578–87.
24. Donati I, Stredanska S, Silvestrini G, Vetere A, Marcon P, Marsich E, et al. The aggregation of pig articular chondrocyte and synthesis of extracellular matrix by a lactose-modified chitosan. Biomaterials. 2005;26:987–98.
25. Donati I, Travan A, Pelillo C, Scarpa T, Coslovi A, Bonifacio A, et al. Polyol synthesis of silver nanoparticles: mechanism of reduction by alditol bearing polysaccharides. Biomacromolecules. 2009;10:210–3.
26. Brambilla E, Ionescu A, Gagliani M, Cochis A, Arciola CR, Rimondini L. Biofilm formation on composite resins for dental restorations: an in situ study on the effect of chlorhexidine mouthrinses. Int J Artif Organs. 2012;35:792–9.
27. Moura LIF, Dias AMA, Carvalho E, de Sousa HC. Recent advances on the development of wound dressings for diabetic foot ulcer treatment—a review. Acta Biomater. 2013;9:7093–114.
28. Travan A, Marsich E, Donati I, Benincasa M, Giazzon M, Felisari L, et al. Silver-polysaccharide nanocomposite antimicrobial coatings for methacrylic thermosets. Acta Biomater. 2011;7:337–46.
29. Kong M, Chen XG, Xing K, Park HJ. Antimicrobial properties of chitosan and mode of action: a state of the art review. Int J Food Microbiol. 2010;144:51–63.
30. Morones JR, Elechiguerra JL, Camacho A, Holt K, Kouri JB, Ramírez JT, et al. The bactericidal effect of silver nanoparticles. Nanotechnology. 2005;16:2346–53.
31. Xiu Z, Zhang Q, Puppala HL, Colvin VL, Alvarez PJJ. Negligible particle-specific antibacterial activity of silver nanoparticles. Nano Lett. 2012;12:4271–5.
32. Silva JM, Georgi N, Costa R, Sher P, Reis RL, Van Blitterswijk CA, et al. Nanostructured 3D constructs based on chitosan and chondroitin sulphate multilayers for cartilage tissue engineering (Barbosa MA, editor). PLoS One. 2013;8:e55451.
33. Barui A, Khare R, Dhara S, Banerjee P, Chatterjee J. Ex vivo biocompatibility of honey-alginate fibrous matrix for HaCaT and 3T3 with prime molecular expressions. J Mater Sci Mater Med. 2014;25:2659–67.
34. Lee Y-H, Cheng F-Y, Chiu H-W, Tsai J-C, Fang C-Y, Chen C-W, et al. Cytotoxicity, oxidative stress, apoptosis and the autophagic effects of silver nanoparticles in mouse embryonic fibroblasts. Biomaterials. 2014;35:4706–15.